PHYSICAL REVIEW A, VOLUME 63, 030702(R)

# Experimental observation of non-Coulombic states of transient multicharged molecular ions $N_2^{4+}$ and $O_2^{4+}$

C. Cornaggia and L. Quaglia
*CEA Saclay, Division des Sciences de la Matière, Service des Photons, Atomes et Molécules, Bâtiment 522, F-91191 Gif-sur-Yvette, France*

(Received 28 July 2000; published 7 February 2001)

A direct experimental evidence of non-Coulombic states of $N_2^{4+}$ and $O_2^{4+}$ transient multicharged ions is presented using laser-induced Coulomb explosion and kinetic-energy spectra measurements of, respectively, the $N^{2+}+N^{2+}$ and $O^{2+}+O^{2+}$ fragmentation channels. The substructure patterns of the energy spectra provide an unambiguous identification of several fragmentation channels within the same final charge states of the fragments. Higher laser intensities favor higher energetic channels. This experimental fact and *ab initio* calculations from the literature indicate that the molecule explodes at an internuclear distance range close to the equilibrium internuclear distance for these high energetic channels.

DOI: 10.1103/PhysRevA.63.030702 PACS number(s): 33.80.Rv, 33.80.Eh, 42.50.Vk

The laser-induced Coulomb explosion of molecules is an expanding field of research due to the fast progress of ultrashort-pulse laser technologies and nonperturbative theoretical approaches of the laser-molecule interaction [1]. The common feature of the intense laser excitation with other types of excitation sources is the multifragmentation of undetected transient multicharged molecules. In the case of ion-impact-induced fragmentation of molecules [2,3], a simple Coulomb explosion model is insufficient to explain the measured fragmentation energies, for instance in $H_2O$ for the $H^+ + O^{Z+} + O^+$ $(Z=1-4)$ channels [2]. The experimental data are interpreted in terms of non-Coulombic dissociative electronic states of the corresponding multicharged molecular ions. In experiments performed with femtosecond lasers, the interaction time is of the order of the pulse duration, several tens of femtoseconds, and is much longer than the interaction time in fast-ion-impact or beam-foil experiments, typically a fraction of one femtosecond [2–4]. In consequence, the molecule has enough time to stretch out during the laser interaction. In most of the nonpertubative models, the weaker than expected kinetic-energy releases from a simple Coulomb explosion are explained by an enhancement of the multiple ionization process at some critical distance larger than the equilibrium one [5–8]. Until now, non-Coulombic electronic states of multicharged molecular ions have never been detected using the intense laser excitation for fragmentation channels involving multicharged atomic fragments. This Rapid Communication is aimed at reporting experimental evidence of the presence of these states for two simple molecules $N_2$ and $O_2$. These results are of importance for Coulomb explosion imaging techniques, since the position coordinates of the molecular system are deduced from the momenta of the fragments. Indeed, a precise knowledge of the potential repulsion curves is necessary to calculate the position coordinates from the momenta measurements [9,10].

A molecular explosion following a particular channel, for instance, $AB^{(Z+Z')+} \rightarrow A^{Z+} + B^{Z'+}$ for a diatomic molecule, gives fragments' momentum distributions $D(\mathbf{p})$ that can be written in the case of a linearly polarized laser field along the $Oz$ axis as follows:

$$D(\mathbf{p}) = D(p_x, p_y, p_z) = F(p, \theta), \tag{1}$$

due to the cylindrical symmetry around the $Oz$ axis. In Eq. (1), the momentum distribution depends only on the modulus $p$ and angle $\theta$ with the $Oz$ axis of the momentum vector $\mathbf{p}$. If several electronic states of the transient multicharged molecular ion $AB^{(Z+Z')+}$ contribute to the dissociation channel, then several local maxima $p_i$ are expected in the distribution $F(p,\theta)$. In this work, we use a Wiley-McLaren ion time-of-flight spectrometer [11] that allows one to get the ionic fragment momentum $p_Z$ along the spectrometer axis $OZ$ following:

$$p_Z = -qF_c(t - t_0), \tag{2}$$

where $q$ and $F_c$ are, respectively, the charge of the ion and the collection electric field, and $t$ and $t_0$ are, respectively, the time of flight of the ion and the time of flight of the same ion with zero momentum $p_Z = 0$ along the spectrometer axis. If the laser-electric-field axis $Oz$ is equal to the axis of the ion spectrometer $OZ = Oz$, then the measurement of the time-of-flight spectrum is equivalent to the measurement of the distribution $D_{\mathrm{Meas}}(p_z)$:

$$D_{\mathrm{Meas}}(p_z) = \int\int dp_x dp_y \, A(p_x, p_y)\, D(p_x, p_y, p_z), \tag{3}$$

where $A(p_x, p_y)$ is the acceptance function of the overall detection of the ion spectrometer as a function of $p_x$ and $p_y$. Taking advantage of the cylindrical symmetry of the fragmentation in Eq. (1) and of the ion spectrometer, the distribution $D_{\mathrm{Meas}}(p_z)$ can be written as:

$$D_{\mathrm{Meas}}(p_z) = \pi p_z^2 \int_0^\infty du \, A(p_z\sqrt{u})\, F\left(p = p_z\sqrt{1+u},\ \theta = \tan^{-1}(\sqrt{u})\right), \tag{4}$$

where the variable $u$ is given by $u = (p_x^2 + p_y^2)/p_z^2$. The main consequence of Eq. (4) is that the measured momentum spectrum $D_{\mathrm{Meas}}(p_z)$ gives a complicated convolution of the

 

initial physical distribution $F(p,\theta)$ including the angular distribution of the ejected fragments with the aperture function $A(p_x,p_y)$. The aim of this work is to get a direct measure of the $F(p,\theta=0)$ at $\theta=0$ without any contribution of the total angular distribution using a simple experimental procedure.

For the sake of clarity, we present kinetic-energy spectra $S_{\mathrm{Meas}}(E_z)$ normalized to the energy $E_z=p_z^2/(2m)$ following $S_{\mathrm{Meas}}(E_z)\,dE_z=D_{\mathrm{Meas}}(p_z)\,dp_z$, where $m$ is the ion mass. In what follows, the energy denomination always means the $E_z$ value, which is measured following Eq. (2). Two types of kinetic-energy spectra are used for a particular ion $A^{Z+}{}_d$, where the subscript $d$ means the direction $d=f$ (*forward*) or $d=b$ (*backward*) of the emitted fragment relative to the detector position. The first comes from the usual time-of-flight spectrum, where all the ions $A^{Z+}{}_d$ are detected without any identification of their companion ion $B^{Z'+}{}_{d'}$ within the same fragmentation channel $A^{Z+}+B^{Z'+}$. The second type of energy spectrum is based on the covariance coefficient $C_2(A^{Z+}{}_d,B^{Z'+}{}_{d'})$ [12,13] and represents the kinetic-energy spectrum of ions $A^{Z+}{}_d$, which belong to the $A^{Z+}{}_d+B^{Z'+}{}_{d'}$ fragmentation channel, with $d'\neq d$ for momentum conservation reasons. Finally, the accuracy of the $p_z$ measurements following Eq. (2) is limited by the initial molecular Maxwell-Boltzmann velocity distribution. For a fragment ejected with a mono-kinetic-energy distribution at $E=E_{\mathrm{F}}$ in the molecular frame of a homonuclear diatomic molecule, the kinetic-energy distribution in the laboratory frame is no longer a mono-kinetic-energy distribution, but presents a broadening given by $\sqrt{2\ln(2)E_F kT}$ for the half width at half maximum (HWHM), where $k$ is the Boltzmann constant, $T$ is temperature, and $kT\ll E_F$. At room temperature $kT=0.026$ eV, the resolution is given by $\Delta E=\pm 0.73$ eV for a fragment with initial energy $E_{\mathrm{F}}=15$ eV, which is representative of the energies reported in this work.

The experimental setup involves two Wiley-McLaren ion spectrometers built in the opposite directions of the *same* laser-molecule interaction region limited by two 90%-high-transparency grids. The parallel grids are separated by 20 mm and present a 80-mm-diam aperture fixed on 120-mm-diam thin electrodes. The 40-fs laser pulses are focused by an $F=+75$ mm on-axis parabolic mirror. Depending on the direction of the collection electric field $F_c$, the ionic fragments can be sent to the first *exclusive—or* to the second ion spectrometer. The first ion spectrometer has a short 120-mm-long drift tube, in order to detect all the fragments without any angular discrimination taking advantage of the molecular reorientation by the intense laser field. Figures 1(a) and 1(b) represent the kinetic-energy spectra of, respectively, all the $N^{2+}{}_f$ ions emitted toward the detector in the Coulomb explosion of $N_2$, and of the $N^{2+}{}_f$ ions that belong to the $N^{2+}{}_f+N^{2+}{}_b$ fragmentation channel. As expected, the ion peak at 7 eV in Fig. 1(a) is missing in the $N^{2+}{}_f+N^{2+}{}_b$ covariance spectrum of Fig. 1(b), since this peak is due to the $N^{2+}{}_f+N^{+}{}_b$ fragmentation channel.

The second ion spectrometer is built with a long 780-mm-long drift tube. In this case, a strong angular discrimination

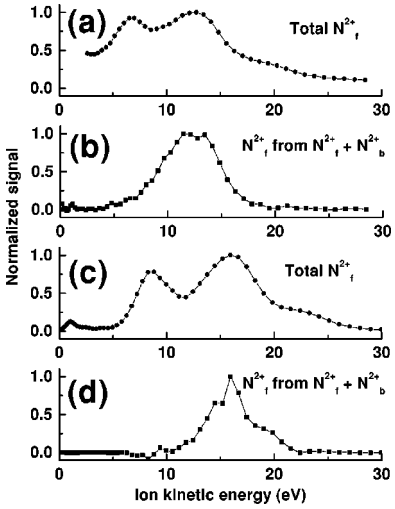


FIG. 1. Kinetic-energy spectra of $N^{2+}{}_f$ ions of $N_2$ recorded at $I=4\times10^{15}$ W/cm$^2$ and $\lambda=800$ nm. Total (a) and covariance (b) spectra recorded with the short drift-tube spectrometer at $p(N_2)=1.2\times10^{-9}$ Torr, and total (c) and covariance (d) spectra recorded with the long drift-tube spectrometer at $p(N_2)=2.2\times10^{-9}$ Torr. In each case, the laser electric field is parallel to the spectrometer axis and the collection electric field is $F_c=100$ V.

allows one to detect only fragments ejected along the spectrometer axis. Figures 1(c) and 1(d) represent kinetic-energy spectra recorded using exactly the same conditions as in Figs. 1(a) and 1(b), respectively. The first important result of Figs. 1(c) and 1(d) is an overall shift of several electron volts toward higher kinetic energies, when ions are detected along the spectrometer axis. The origin of this observation comes from the experimental method illustrated in Eq. (4). In the case of the short-drift-tube spectrometer, the acceptance function $A(p\sqrt{u})$ is a constant and the measured momentum distribution, or equivalently the energy distribution, includes a convolution of the angular dependence of the initial distribution $F(p,\theta)$ with all the possible directions of ejection. Simple mathematical arguments show that this convolution shifts the $D_{\mathrm{Meas}}(p_z)$ distribution toward smaller values of $p_z$ in comparison with the momentum modulus $p$ values of the $F(p,\theta=0)$ distribution. In the case of the long-drift-tube ion spectrometer, the acceptance function $A(p\sqrt{u})$ is a narrow top-hat function, and Eq. (4) gives

$$D_{\mathrm{Meas}}(p_z)=A_0\,\pi\theta_d^2\,p_z^2F(p=p_z,\theta=0)\,, \tag{5}$$

where $A_0$ is a constant lower than 1 that takes into account the ion detection efficiency, and $\theta_d$ is the maximum small angle of detection. Only, in this case, the measured momentum spectrum gives directly the physical momentum distribution $F(p=p_z,\theta=0)$. In consequence, the results discussed in this Rapid Communication were recorded using this last experimental configuration.

The second important feature of Fig. 1(d) is the occurrence of several structures at 15, 16, and 19 eV. These structures are absent in the total energy spectrum of Fig. 1(c), because in this case all the $N^{2+}{}_f$ ions are detected independently of the kinetic energies of the $N^{+}{}_b$, $N^{2+}{}_b$,

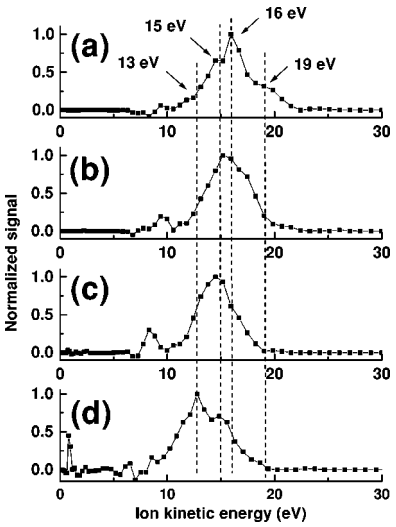


FIG. 2. Kinetic-energy spectra of $N^{2+}{}_f$ ions of $N_2$ from the $N^{2+}{}_f + N^{2+}{}_b$ channel recorded at different laser intensities using the covariance mapping technique and the strong angular discrimination introduced by the long time-of-flight spectrometer: (a) $I=4\times10^{15}$ W/cm$^2$, (b) $I=2\times10^{15}$ W/cm$^2$, (c) $I=1.2\times10^{15}$ W/cm$^2$, (d) $I=6\times10^{14}$ W/cm$^2$.

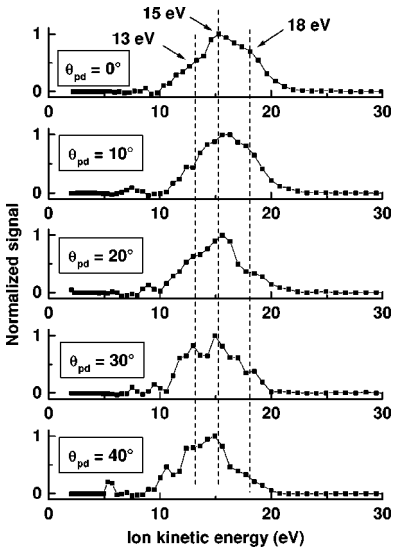


FIG. 3. Kinetic-energy spectra of $O^{2+}{}_f$ ions of $O_2$ from the $O^{2+}{}_f + O^{2+}{}_b$ channel recorded at different laser polarization directions using the covariance mapping technique and the strong angular discrimination introduced by the long time-of-flight spectrometer. The angle $\theta_{pd}$ is the angle between the laser polarization direction and the spectrometer axis, and is indicated for each energy spectrum. The laser intensity $I=4\times10^{15}$ W/cm$^2$ is the same for the five spectra.

and $N^{3+}{}_b$ companion fragments. In this last case, the addition of the overlapping kinetic-energy distributions from all the $N^{2+}{}_f + N^{Z+}{}_b$ $(Z=1,2,3)$ fragmentation channels cancels the substructures due to a particular channel. These structures come from several kinetic-energy releases at 30, 32, and 38 eV for the same $N^{2+}+N^{2+}$ fragmentation channel. The most straightforward interpretation of this result is that several non-Coulombic electronic states of the transient $N_2{}^{4+}$ contribute to the $N^{2+}+N^{2+}$ dissociation channel. Indeed, Safvan and Mathur have calculated two electronic states of this transient molecular ion that dissociate via the $N^{2+}(^2P)+N^{2+}(^4P)+34.9$ eV for the $^5\Sigma_u^+$ state, and $N^{2+}(^2P)+N^{2+}(^2P)+42.5$ eV for the $^3\Sigma_g^-$ state, if the dissociation begins at the neutral equilibrium distance $R_e=1.098$ Å [9]. Another calculation performed by Remscheid *et al.* is in good agreement with the energies of Safvan and Mathur [3]. The highest energy peaks in Fig. 1(d) give total kinetic-energy releases of 32 and 38 eV that are not too far from the calculated energies. Figures 2(a)–2(d) represent the dependence of the covariance kinetic-energy spectra with the peak laser intensity. For low laser intensities, a shift of the overall spectrum toward smaller kinetic energies is observed. However, this shift is not a continuous one, but comes from different contributions of the substructure peaks at different laser intensities. For instance, in Fig. 2(c), the substructure at 19 eV disappears at $1.2\times10^{15}$ W/cm$^2$, while the peak at 15 eV remains the strongest one. In Fig. 2(d) at $6\times10^{14}$W/cm$^2$, this last peak is dominated by the peak at 13 eV, which appears as a shoulder subpeak at higher laser intensities.

The presence of substructures is not a specificity of the $N^{2+}+N^{2+}$ fragmentation channel in $N_2$, but is also observed for other channels in $N_2$ and $O_2$ with identical laser intensity dependences. A longer report will be presented later. Another example is illustrated in Fig. 3, which represents different kinetic-energy spectra of the $O^{2+}{}_f$ ion from the $O^{2+}{}_f + O^{2+}{}_b$ fragmentation channel at different angles between the laser polarization and spectrometer axis directions. These kinetic-energy spectra are recorded using the same $I=4\times10^{15}$ W/cm$^2$ laser intensity. For each spectrum presented in Fig. 3, substructures at 13, 15, and 18 eV are clearly observed. The lack of calculations of $O_2{}^{4+}$ potential curves do not allow a comparison as in the $N_2$ case. When the angle between the laser polarization and spectrometer axis directions is increased, the overall substructure pattern remains observable, with a slight decrease of the substructure at 18 eV and an increase of the substructure at 13 eV. This effect is linked to the laser intensity dependence illustrated in Fig. 2. Indeed, the long-time-of-flight detection allows one to detect molecular explosions for molecules aligned along the spectrometer axis. When the laser polarization is not parallel to this detection axis, the signal comes from molecules that have been not completely reoriented. These molecules have a higher probability to explode in the rising edge of the laser pulse, and in consequence do not experience the maximum laser field. Otherwise, they should be reoriented along the laser electric field, and in consequence should not be detected.

In conclusion, the detection of substructure patterns in the kinetic-energy spectra recorded with $N_2$ and $O_2$ is a clear signature of non-Coulombic electronic states of the corresponding multicharged molecular ions. Higher laser intensities favor higher kinetic-energy releases, and indicate that the molecular explosion occurs at internuclear distances closer to the equilibrium distance. For the $N^{2+}+N^{2+}+E_{\mathrm{Kin}}$ channel corresponding to the transient $N_2{}^{4+}$ ion, the highest energies

at $E_{\mathrm{Kin}}=38$ eV and $E_{\mathrm{Kin}}=32$ eV are not too far from *ab initio* calculations at the equilibrium distance. Lower kinetic-energy releases $E_{\mathrm{Kin}}$ dominate at lower laser intensities and may be due to enhanced ionization at larger internuclear distances [5–8].

The authors are pleased to acknowledge G. Vigneron (CEA/DRECAM/SCM) for his expertise of the kHz laser facility, and M. Bougeard and E. Caprin for their skilled technical assistance. This work is partly supported by INTAS, Grant No. 99-01495.

[1] S. Chelkowski, P. B. Corkum, and A. D. Bandrauk, Phys. Rev. Lett. **82**, 3416 (1999).
[2] U. Werner, K. Beckord, J. Becker, H. O. Folkerts, and H. O. Lutz, Nucl. Instrum. Methods Phys. Res. B **98**, 385 (1995).
[3] A. Remscheid, B. A. Huber, P. Pykavyj, V.Staemmler, and K. Wiesemann, J. Phys. B **29**, 515 (1996).
[4] Z. Vager, R. Naaman, and E. P. Kanter, Science **244**, 426 (1985).
[5] J. H. Posthumus, L. J. Frasinski, A. J. Giles, and K. Codling, J. Phys. B **28**, L349 (1995).
[6] T. Zuo and A. D. Bandrauk, Phys. Rev. A **52**, R2511 (1995).
[7] S. Chelkowski, T. Zuo, O. Atabek, and A. D. Bandrauk, Phys. Rev. A **52**, 2977 (1995).
[8] T. Seideman, M. Yu. Ivanov, and P. B. Corkum, Phys. Rev. Lett. **75**, 2819 (1995).
[9] C. P. Safvan and D. Mathur, J. Phys. B **27**, 4073 (1994).
[10] A. D. Bandrauk, D. G. Musaev, and K. Morokuma, Phys. Rev. A **59**, 4309 (1999).
[11] W. C. Wiley and I. H. McLaren, Rev. Sci. Instrum. **26**, 1150 (1955).
[12] L. J. Frasinski, K. Codling, and P. A. Hatherly, Phys. Lett. A **142**, 499 (1989).
[13] Ph. Hering and C. Cornaggia, Phys. Rev. A **59**, 2836 (1999).